Transactions, SMiRT-25
Charlotte, NC, USA, August 4-9, 2019
Division VIII

Monitoring Alkali Silica Reaction Of Large And Medium-scale Concrete Specimens Using Acoustic Emission

Vafa Soltangharaei[1], Rafal Anay[1], Li Ai[1], Yann Le Pape[2], Zhongguo John Ma[3], Paul Ziehl[4]

[1] Research assistant, Civil and Environmental Engineering Department, University of South Carolina, Columbia, SC, USA (vafa @email.sc.edu)
[2] Senior Scientist, Oak Ridge National Laboratory, Oak Ridge, TN, USA (lepapeym@ornl.gov)
[3] Professor, Department of Civil and Environmental Engineering, University of Tennessee, Knoxville, TN, USA (zma2@utk.edu)
[4]Professor, Civil and Environmental Engineering Department, University of South Carolina, Columbia, SC, USA (ziehl@cec.sc.edu)

ABSTRACT

Alkali-silica reaction (ASR) causes cracks in civil concrete structures such as nuclear power plants and may endanger their serviceability and integrity. The damage caused by ASR in the nuclear structures initiates mainly inside the structure and appears later on the surface. Acoustic emission (AE) is a passive method to monitor structural health. It is also is very sensitive and has the capability of monitoring continuously. This method may be an alternative for early damage detection in concrete nuclear structures affected by ASR. In this study, ASR was monitored by acoustic emission in both large-scale and medium-scale concrete structures. The expansion strains are measured and calculated in order to compare them with the AE data. The confinement causes anisotropic expansion and stress redistribution. Larger AE activity is observed in the confined specimens.

INTRODUCTION

Concrete is one of the common materials in civil engineering constructions. However, its brittle mechanical characteristic makes it vulnerable to crack formation. One of the main cracking sources in the concrete structures is alkali-silica reaction (ASR). ASR is a chemical reaction, which occurs between silica existing in the reactive aggregates and alkaline in the cement. The result is a hygroscopic gel, which tends to imbibe the humidity and expand (Soltangharaei et al. (2018b)). The gel imposes pressure on both aggregates and the cement matrix causing crack formation. The common structures which are exposed to ASR are bridges (Bach et al. (1993) , Bakker (2008) , Clark (1989) , Schmidt et al. (2014)), concrete dams (Campos et al. (2018) , Plusquellec et al. (2018)), nuclear power plants, and nuclear waste containments (Saouma et al. (2014) , Soltangharaei et al. (2018a) , Takakura et al. (2005) , Tcherner et al. (2009)). Because of the safety and radioprotection functions of concrete structures in nuclear power plant, the effects of ASR and their significance to current and long-term operation must be thoroughly addressed.

There are different methods for monitoring ASR damage and studying its effect on the structures. Some that are traditionally employed for this purpose are: regular-base visual inspection, coring, petrographic analysis, demountable mechanical strain gauge (DEMEC gauge), relative humidity or moisture content measurement, and crack indexing. These methods have several disadvantages. For example, visual inspection would not be effective for early damage detection. ASR reaction appears to

initiate internally in the thick shear walls of nuclear facilities due to in-plane confinement. The resulting cracks appear on the surface at a later stage of the ASR process. In addition, visual inspection for large-scale structures is time-consuming and subject to human error (Rajabipour et al. (2015)). Coring and petrographic analyses are destructive methods and commonly unpractical for sensitive structures such as nuclear power plants. In addition, it is difficult to evaluate the entire condition of a structure by taking only a few cores or samples. DEMEC gauge and expansion measurement work for measuring the diameter of piles, but it is not a satisfactory method for thick concrete walls since most of the expansion occurs out of the plane, and only one side of the walls is usually accessible.

The potential alternatives for structural health monitoring are non-destructive test methods. One non-destructive health monitoring method is acoustic emission (AE). This method uses highly sensitive piezoelectric AE sensors to record the elastic stress waves emitted during the formation of cracks. This method is very sensitive and can monitor structures continuously without halting operation. AE has been previously employed as a structural health monitoring system in different structures and materials (Colombo et al. (2003) , Droubi et al. (2017) , Soltangharaei et al. (2018a) , Soltangharaei et al. (2019)). In addition, it has been used to monitor the physical effects of chemical reactions such as corrosion, hydration, and ASR (Abdelrahman et al. (2018) , Abdelrahman et al. (2015) , Assi et al. (2018) , Farnam et al. (2015)).

Recently, there have been several investigations conducted where AE was applied for the detection of damage and the quantification of the defects caused by ASR (Abdelrahman et al. (2015) , Farnam et al. (2015) , Lokajíček et al. (2017) , Weise et al. (2012)). Farnam et al. (2015) utilized peak frequency and frequency centroid to characterize signal signatures that emanate from cracks in aggregates and cement paste. High-frequency signals were observed in the earlier stage of ASR, while the low-frequency signals appeared later in the ASR process. X-ray images helped the authors to verify their hypothesis. Lokajíček et al. (2017) utilized both ultrasonic pulse velocity and AE to monitor the damage caused by ASR. Four specimens with different aggregate reactivities were used. The variation of cumulative energy correlated with the damage level and ultrasonic results. All mentioned researches have used small-scale specimens such as standard mortar bars or concrete prisms with a maximum dimension of 12 inches. These specimens did not have any reinforcement or confinement. In this study, medium and large-scale specimens affected by ASR have been monitored by AE. The specimens have steel reinforcement and confinement. Therefore, the confinement effect on the damage pattern is investigated. The expansion strains have been measured on a regular basis and utilized to compare with the AE data. AE cumulative signal strength (CSS) and historic index (HI) are used to study the ASR expansion effects on the AE activities.

TEST SETUP

In total, six concrete specimens (three large-scale and three medium-scale) were cast for the ASR test. The large-scale concrete blocks have the dimensions of 3.5 m (length) × 3 m (width) × 1 m (height). Two specimens had reactive aggregates (reactive specimens), and one has LiNO3 to stop ASR reaction. All of the large-scale specimens had steel reinforcement meshes at top and bottom including US # 11 spaced 25.4 cm. One of the reactive specimens was enclosed by a rigid steel frame to prevent the specimen from in-plane expansion. This specimen referred to as the “confined large-scale specimen”. The other reactive specimen did not have an encasement in the plane. This specimen is referred to as the “unconfined large-scale specimen”. The non-reactive specimen is referred to as the “control large-scale specimen”. Alkali-tolerant strain transducers and long-gauge fiber extensometers were employed for expansion measurements along with different dimensions. Seven AE sensors were employed in each reactive specimen. Four of them were resonant sensors and three were broadband sensors. Broadband sensors were WDIUC-AST with an operating frequency range of 200-900 kHz. These were embedded in the specimens before casting. More details about the test setup can be found in (Hayes et al. (2018) , Soltangharaei et al. (2018b)).

Medium-scale specimens include three cubic concrete blocks with the dimensions of 112 cm (length) × 31 cm (width) × 31 cm (height). They were cast at the University of Alabama and transferred to the University of South Carolina for conducting the test. Similar to the large-scale specimens, two specimens have reactive aggregates, which referred to as "reactive specimens". One of the reactive specimens had both longitudinal and transverse reinforcements. Therefore, two dimensions (length and height) of the specimens were partially confined. Four US#7 were employed as longitudinal reinforcements. For transverse reinforcements, US #6 bars were used along the specimen height and spaced by 15.2 cm. This specimen is referred to as the "confined medium-scale specimen". The other reactive specimen does not have any reinforcements and is referred to as the "unconfined medium-scale specimen". The non-reactive specimen does not have reactive aggregates and is referred to as "control medium-scale specimen". Ten broadband AE sensors were attached on each reactive specimen. The sensors were PKWDI with an operating frequency of 200-850 kHz. The schematic picture for the test setup is presented in Figure 1. DEMEC gauges were used for the expansion measurement along the three dimensions. The expansion was measured regularly every month.

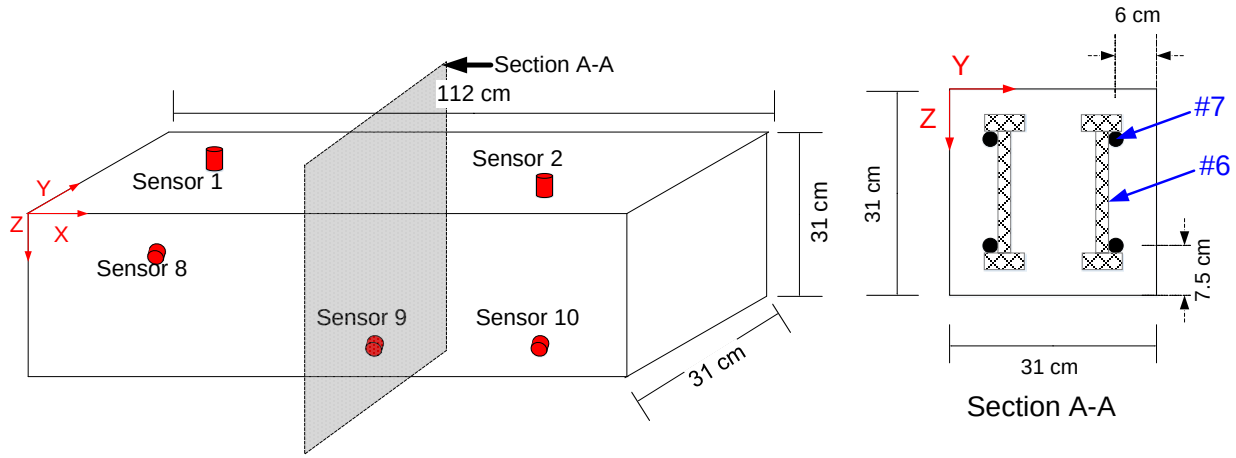

(a) Confined specimen

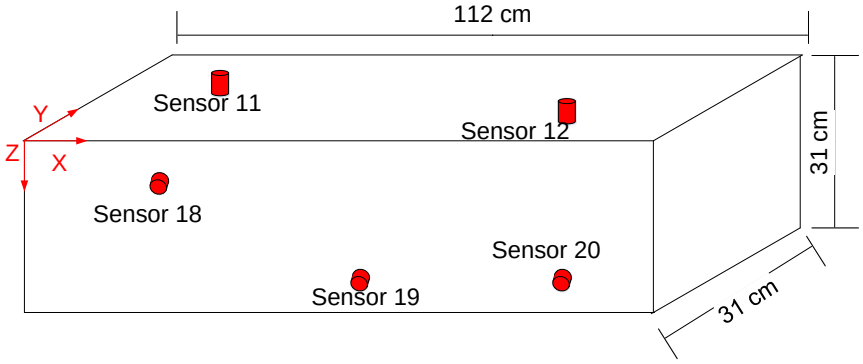

(b) Unconfined specimens

Figure 1 Test setup for medium-scale specimens

The large-scale specimens were conditioned in a high humidity and temperature in a large environmental chamber at the University of Tennessee at Knoxville, and the medium-scale specimens were conditioned in a chamber at the University of South Carolina.

METHODOLOGY

AE data acquired with broadband sensors from both large-scale and medium-scale specimens have been utilized for analyzing. The AE data had non-genuine signals. Therefore, the first step before analyzing the AE data is filtering. The AE data from large-scale specimens had a few false data readings because the broadband sensors were embedded inside the specimens and immune to environmental noises. The duration-amplitude distribution was utilized for filtering the data. The rejection limits were presented in (Soltangharaei et al. (2018b)).

In the medium-scale specimens, some sensors collected a large amount of extraneous data due to faulty connections. A different procedure than for the large-scale specimen was employed to filter the data for these specimens due to a large amount of data produced by noise. Using duration-amplitude for the medium-scale specimens is very time-consuming and expensive. The noises from faulty connections have specific signal features such as a small counts, average frequency, and peak frequency. An example of false and genuine data is shown in Figure 2. Initially, the noises related to the faulty connections were removed by deleting the data with an average frequency lower than 60 kHz. Some faulty data remained from the first stage. Therefore, another filter was applied to the contaminated channel by removing the signals with a peak frequency of less than 80 kHz. The filtering procedure mentioned above removed a large amount of data produced by noise. Then, the events which include at least four hits were kept, and the rest of the data was filtered.

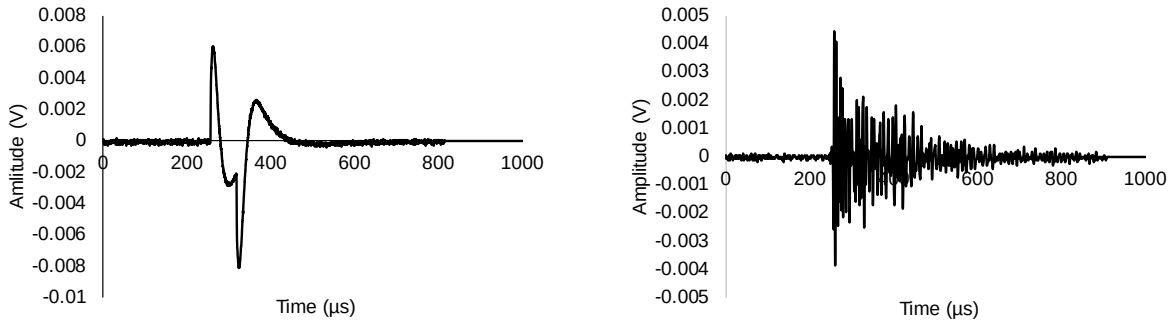

(a) Faulty connection noise (b) Genuine AE data

Figure 2 Genuine versus false AE data

HI is one of the two indices in the intensity analysis. The parameters for intensity analysis are calculated and usually presented on the logarithmic axes. The historic index is related to changes in the rate of cumulative signal strength. In this study, HI values are calculated in terms of the experiment time. The historic index is calculated according to the following equation (Nair et al. (2010)):

$$HI = \frac{N}{N-K}\left(\frac{\sum_{i=k+1}^{N} S_{oi}}{\sum_{i=1}^{N} S_{oi}}\right) \quad (1)$$

where *HI* is historic index; *N* is the number of hits up to the desired experiment time; S_{oi} is signal strength of i^{th} hit in the considered data set; *K* is an empirical constant, which depends on the material, and data density during monitoring.

RESULTS

The strains in different coordinates were measured and presented in Figure 3. As seen in the figure, the strains were named as in-plane and out-of-plane strains. The out-of-plane strain is a strain caused by expansion perpendicular to the plane containing the steel reinforcement meshes. There are two in-plane strains for each specimen: “in-plane strain 1” is strain due to the expansion in the plane containing the steal reinforcement along the larger dimension and “in-plane strain 2” is the strain due to expansion in the plane containing the steal reinforcement along the smaller dimension. For the medium-scale specimens, only the confined specimen has the reinforcement, and out-of-plane direction is defined according to this specimen. The out-of-plane direction is along the Y axis. “In-plane strain 1” is the strain along the X axis and “In-plane strain 2” is along the Z direction (Figure 1). In the large-scale specimen, all the specimens have reinforcement as mentioned in the test setup. The “out-of-plane strain” is the strain due to expansion perpendicular to the reinforcement mesh along the specimen height (thickness) and “in-plane strain 1” is the strain due to expansion in the plane containing the reinforcement mesh along the larger dimension and “in plane strain 2” is the strain due to expansion in the plane containing the reinforcement along the smaller dimension (Soltangharaei et al. (2018b)).

As seen in Figure 3, the out-of-plane expansion for both confined large-scale and medium-scale specimens are larger than corresponding values for the unconfined specimens. ASR expansion and stress are redistributed along the direction with the lower restrain (Liaudat et al. (2018)). This is the reason for larger out-of-plane strain associated with the confined specimens as compared to unconfined specimens.

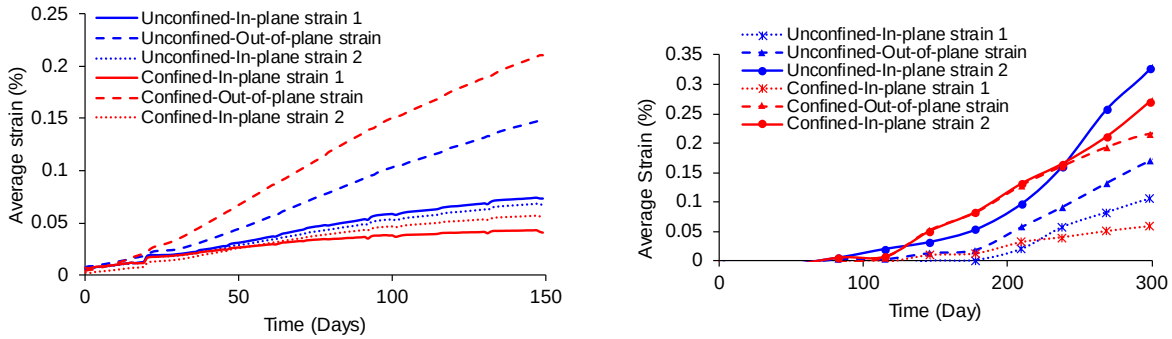

(a) Large-scale specimens (b) Medium-scale specimens

Figure 3 ASR expansion strains (Hayes et al. (2018))

In the medium-scale specimen, the values for in-plane strain 2, for both confined and unconfined specimens, are the largest during the experiment. In the confined specimen, in-plane strain 2 has an almost similar value as the out-of-plane strain. Expansion along with the height of the specimens account for the in-plane strain 2. The casting was conducted parallel to this direction. The researchers have shown a significant effect of casting direction in the anisotropic expansion caused by ASR (Smaoui et al. (2004)). This effect is observed from the strain measurements in the medium-scale specimens. Although the confined specimen had confinement along the height of the specimen, the largest strains still occur in this direction.

In the large-scale specimens, the casting direction is perpendicular to the confinement plane. Therefore, in addition to the confinement effect, the casting also influences the out-of-plane strains.

The in-plane strain 1 in the confined medium-scale specimen is more than the strain for the unconfined specimen up to 210 days. After 210 days, the in-plane strain 1 for the unconfined specimen

increases and its values become larger than the values for the confined specimen. The confinement for the confined specimen controls the expansion in this direction.

Figure 4 shows the cracking on the top surface of the medium-scale specimen after the test. The cracks in the confined specimen are more anisotropic than the crack pattern in the unconfined. The cracks mostly align the larger dimension, parallel to the reinforcement plane (X-Z plane). However, the crack pattern in the unconfined specimen is randomly distributed in both directions on the top surface of the specimen. The difference between the crack patterns shows the effect of anisotropic expansion imposed by the confinement in the medium-scale specimens.

(a) Confined specimen

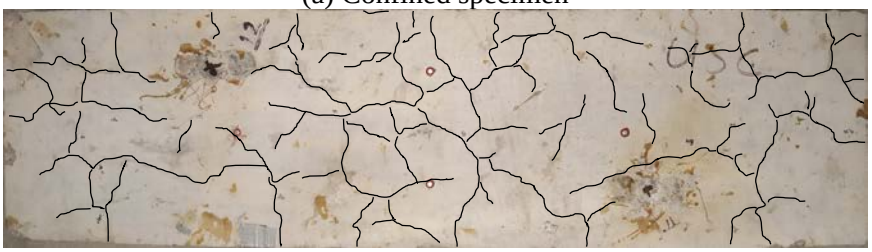

(b) Unconfined specimen

Figure 4 Crack pattern in the medium-scale specimens

The AE data for the large-scale specimens were presented in terms of cumulative signal strength (CSS) in Figure 5. In addition, the out of plane strain is also presented there as well. As seen in Figure 5, the CSS for the confined specimens (large-scale and medium-scale specimens) is much more than the values for the unconfined specimens. As mentioned, the out-of-plane strain for the confined specimens are more than the unconfined specimens. The resulting expansion anisotropy due to ASR causes stress concentration in the confined specimen and consequently more AE activity and the AE with stronger signal strength. In the medium-size specimen, the anisotropy due to confinement reflects more in AE data than the large-scale specimens. This may be due to a larger concentration of AE sensor in a smaller region.

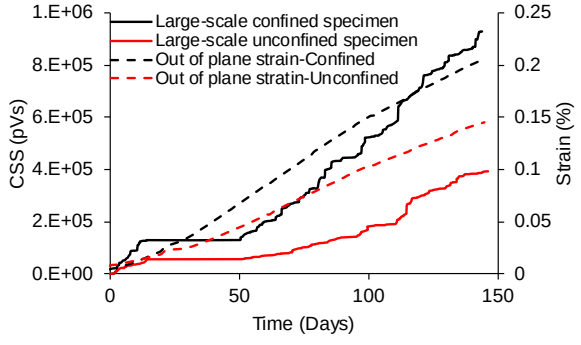

(a) Large-scale specimens

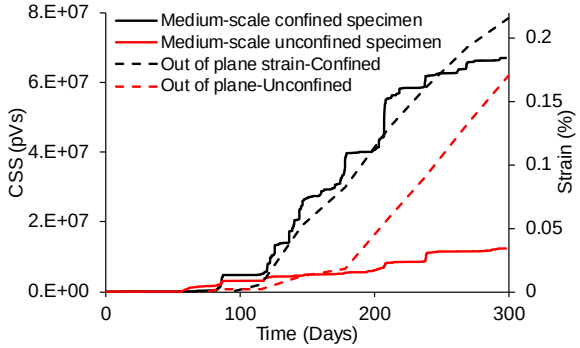

(a) Medium-scale specimens

Figure 5 Cumulative signal strength and out-of-plane strain in terms of time (Hayes et al. (2018))

Historic Index (HI) values were calculated according to Eq. 1 in terms of time, and the maximum HI values up to the desired times are presented in Figure 6. For both specimens, the HI values decrease as the ASR progresses. In other words, the AE events with a large signal strength are decreasing as the ASR continues. Moreover, the HI values for the confined specimens are larger than the HI values of the unconfined specimen. This also indicates the effect of anisotropic expansion due to the confinement on the specimen.

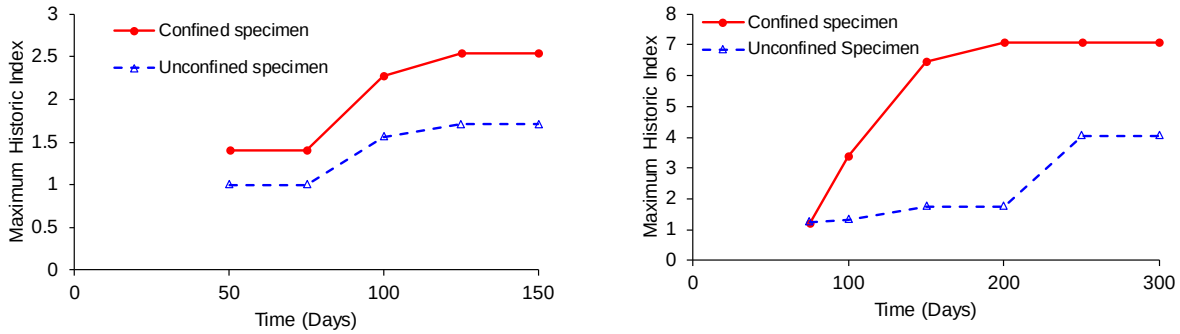

(a) Large-scale specimen (b) Medium-scale specimen

Figure 6 Historic Index versus Time

In the large-scale specimens, the HI trends are similar, and they correlate with the strain's values. The rate of change in the HI values starts to decrease when the strain rate decreases at 100 days. In the confined medium-scale specimen, the HI values increase with a higher rate than the unconfined specimen up to 150 days and starts to decrease after that. In the unconfined medium-scale specimen, the HI rate increases at 200 Days, although its values are still smaller than the values for the confined specimen. This trend is correlated with the strain rate for this specimen that starts to increase around 200 days.

CONCLUSION

In this study, AE has been utilized to monitor the specimens affected by ASR with different scales. Expansion strains along the dimensions of the specimens were measured and calculated. Observing the condition of the medium-scale specimens shows the effect of the anisotropic expansion due to reinforcement confinement. The crack directions in the confined specimen align with a direction parallel to the specimen length. However, the crack pattern for the unconfined specimen is more random and uniformly distributed. This anisotropy in expansion causes a larger AE activity in the confined specimen. The rate of CSS for the confined specimen is larger at the beginning and decreases after that, while the rate of CSS increases after 200 days. This behaviour correlates with the strain rate in the unconfined specimen, which increases after 200 days.

The strain along the height of confined medium-scale specimen is the largest value although this dimension was confined by the transverse reinforcements. This is due to an effect of the casting direction in ASR expansion. The weak layers perpendicular to the casting direction were formed in the specimen during casting. This factor seems to be controlling and should be considered in the damage evaluation.

Comparing the AE results between the large-scale and medium-scale specimens, it shows that the AE activity trends, and energy values are influenced by the boundary condition and dimensions of the specimens, sensor layout, and sensor number.

ACKNOWLEDGEMENT

This material is based upon the work partially supported by the U.S. Department of Energy – Nuclear Energy University Program (NEUP) under the contract DE-NE0008544, the U.S Department of Energy, Office of Nuclear Energy, Light Water Reactor Sustainability Program under contact number DE-AC05-00OR22725, and the U.S Department of Energy Office of Science, Office of Basic Energy Sciences and Office of Biological and Environmental Research and EPSCoR (Established Program to Simulate Competitive Research) under the contract number DE-SC-0012530.

REFERNCES

Abdelrahman, M., ElBatanouny, M., Dixon, K., Serrato, M. and Ziehl, P. (2018). "Remote Monitoring and Evaluation of Damage at a Decommissioned Nuclear Facility Using Acoustic Emission," *Applied Sciences* 8(9), 1663.

Abdelrahman, M., ElBatanouny, M. K., Ziehl, P., Fasl, J., Larosche, C. J. and Fraczek, J. (2015). "Classification of alkali–silica reaction damage using acoustic emission: A proof-of-concept study," *Construction Building Materials* 95, 406-413.

Assi, L., Soltangharaei, V., Anay, R., Ziehl, P. and Matta, F. (2018). "Unsupervised and supervised pattern recognition of acoustic emission signals during early hydration of Portland cement paste," *Cement Concrete Research* 103, 216-225.

Bach, F., Thorsen, T. S. and Nielsen, M. (1993). "Load-carrying capacity of structural members subjected to alkali-silica reactions," *Construction Building Materials* 7(2), 109-115.

Bakker, J. (2008). "Control of ASR related risks in the Netherlands". *Proceedings of the 13th International Conference on Alkali-Aggregate Reaction in Concrete, Trondheim, Norway*, 16-20.

Campos, A., Lopez, C. M., Blanco, A. and Aguado, A. (2018). "Effects of an internal sulfate attack and an alkali-aggregate reaction in a concrete dam," *Construction Building Materials* 166, 668-683.

Clark, L. (1989). Critical review of the structural implications of the alkali silica reaction in concrete. Crowthone, UK, Transportation and Road Research Laboratory.

Colombo, I. S., Main, I. and Forde, M. (2003). "Assessing damage of reinforced concrete beam using “b-value” analysis of acoustic emission signals," *Journal of Materials in Civil Engineering* 15(3), 280-286.

Droubi, M. G., Faisal, N. H., Orr, F., Steel, J. A. and El-Shaib, M. (2017). "Acoustic emission method for defect detection and identification in carbon steel welded joints," *Journal of Constructional Steel Research* 134, 28-37.

Farnam, Y., Geiker, M. R., Bentz, D. and Weiss, J. (2015). "Acoustic emission waveform characterization of crack origin and mode in fractured and ASR damaged concrete," *Cement and Concrete Composites* 60, 135-145.

Hayes, N. W., Gui, Q., Abd-Elssamd, A., Le Pape, Y., Giorla, A. B., Le Pape, S., Giannini, E. R. and Ma, Z. J. (2018). "Monitoring Alkali-Silica Reaction Significance in Nuclear Concrete Structural Members," *Journal of Advanced Concrete Technology* 16(4), 179-190.

Liaudat, J., Carol, I., López, C. M. and Saouma, V. E. (2018). "ASR expansions in concrete under triaxial confinement," *Cement Concrete Composites* 86, 160-170.

Lokajíček, T., Přikryl, R., Šachlová, Š. and Kuchařová, A. (2017). "Acoustic emission monitoring of crack formation during alkali silica reactivity accelerated mortar bar test," *Engineering geology* 220, 175-182.

Nair, A. and Cai, C. (2010). "Acoustic emission monitoring of bridges: Review and case studies," *Engineering Structures* 32(6), 1704-1714.

Plusquellec, G., Geiker, M. R., Lindgård, J. and De Weerdt, K. (2018). "Determining the free alkali metal content in concrete–Case study of an ASR-affected dam," *Cement and Concrete Research* 105, 111-125.
Rajabipour, F., Giannini, E., Dunant, C., Ideker, J. H. and Thomas, M. D. (2015). "Alkali–silica reaction: current understanding of the reaction mechanisms and the knowledge gaps," *Cement and Concrete Research* 76, 130-146.
Saouma, V. E. and Hariri-Ardebili, M. A. (2014). "A proposed aging management program for alkali silica reactions in a nuclear power plant," *Nuclear Engineering Design* 277, 248-264.
Schmidt, J. W., Hansen, S. G., Barbosa, R. A. and Henriksen, A. (2014). "Novel shear capacity testing of ASR damaged full scale concrete bridge," *Engineering Structures* 79, 365-374.
Smaoui, N., Bérubé, M.-A., Fournier, B. and Bissonnette, B. (2004). "Influence of specimen geometry, orientation of casting plane, and mode of concrete consolidation on expansion due to ASR," *Cement, concrete aggregates* 26(2), 1-13.
Soltangharaei, V., Anay, R., Assi, L., Ziehl, P. and Matta, F. (2018a). "Damage identification in cement paste amended with carbon nanotubes". *AIP Conference Proceedings*, AIP Publishing, 030006.
Soltangharaei, V., Anay, R., Begrajka, D., Bijman, M., ElBatanouny, M. K., Ziehl, P. and Van Tooren, M. J. (2019). "A minimally invasive impact event detection system for aircraft movables". *AIAA Scitech 2019 Forum*, 1268.
Soltangharaei, V., Anay, R., Hayes, N., Assi, L., Le Pape, Y., Ma, Z. and Ziehl, P. (2018b). "Damage Mechanism Evaluation of Large-Scale Concrete Structures Affected by Alkali-Silica Reaction Using Acoustic Emission," *Applied Sciences* 8(11), 2148.
Takakura, T., Ishikawa, T., Mitsuki, S., Matsumoto, N., Takiguchi, K., Masuda, Y. and Nishiguchi, I. (2005). "Investigation on the expansion value of turbine generator foundation affected by alkali-silica reaction". *Proceedings of 18th International Conference on Structural Mechanics in Reactor Technology*.
Tcherner, J. and Aziz, T. (2009). "Effects of AAR on seismic assessment of nuclear power plants for life extensions". *Proceedings of the 20th International Conference on Structural Mechanics in Reactor Technology (SMiRT), Espoo, Finland*, 9-14.
Weise, F., Voland, K., Pirskawetz, S. and Meinel, D. (2012). "Innovative measurement techniques for characterising internal damage processes in concrete due to ASR". *Proceedings of the International Conference on Alkali Aggregate Reaction (ICAAR), University of Texas, Austin, TX, USA*, 20-25.